Supplementary Materials for: "Reciprocal polarization imaging of complex media"

Zhineng Xie[a], Weihao Lin[a], Mengjiao Zhu[a], Jianmin Yang[a], Chenfan Shen[a], Xin Jin[a], Xiafei Qian[b] and Min Xu[a,c,*]

[a]Institute of Lasers and Biomedical Photonics, Biomedical Engineering College, Wenzhou Medical University, Wenzhou, Zhejiang, 325035, China.
[b]Chengbei District, Hangzhou First People's Hospital，Hangzhou，Zhejiang，310000，China.
[c]Department of Physics and Astronomy, Hunter College and the Graduate Center, The City University of New York, 695 Park Avenue, New York, NY 10065, USA.

*Corresponding author. Email: minxu@hunter.cuny.edu

Supplementary Text 1: The differences and similarities between Lu-Chipman decomposition and reciprocal polar decomposition

Lu–Chipman decomposition of Mueller matrices was compared with reciprocal polar decomposition for clarity, as shown in Table S1. Lu-Chipman decomposition decomposes the Mueller matrix into a product of three matrices: a depolarizer matrix $\boldsymbol{M}_{\Delta}$, a retarder matrix $\boldsymbol{M}_{R}$, and a diattenuator matrix $\boldsymbol{M}_{D}$ [13, 24, 49], i.e.,

$$\boldsymbol{M} = \boldsymbol{M}_{\Delta}\boldsymbol{M}_{R}\boldsymbol{M}_{D} \tag{S1}$$

Supplementary Text 2: Additional results for fresh beef tissue sections

We also imaged fresh beef tissue sections in serial cuts with thicknesses of 50 μm and 200 μm under identical experimental conditions. The extracted tissue birefringence orientation angle, linear retardance, and depolarization by Lu-Chipman and reciprocal polar decomposition in the backward geometry are shown in Fig. S1. Boxplots are shown in Fig. S2 for the orientation angle,

Table S1. Comparison of the expressions for Lu-Chipman decomposition and reciprocal polar decomposition.

		Lu-Chipman	**Reciprocal polar**
Differences	Application situation	forward and backward	backward
	Expression	$\boldsymbol{M}=\boldsymbol{M_\Delta M_R M_D}$	$\boldsymbol{M}=\boldsymbol{M_D^{\#} M_R^{\#} M_\Delta M_R M_D}$ $\boldsymbol{QM}=\boldsymbol{M_D^T M_R^T M'_{\Delta d} M_R M_D}$
	Symmetric matrix	$\boldsymbol{M}$: No (in general)	$\boldsymbol{QM}$: Yes
	Degrees of freedom	16	10
	$\boldsymbol{M_\Delta}$	$\boldsymbol{M_\Delta}=\begin{bmatrix}1 & \boldsymbol{0^T}\\ \boldsymbol{P_\Delta} & \boldsymbol{m_\Delta}\end{bmatrix}$	$\boldsymbol{M_\Delta}$=diag (d_0, d_1, d_2, d_3)
	$\boldsymbol{M_R}$	$\boldsymbol{M_L M_C}$ or $\boldsymbol{M_C M_L}$	$\boldsymbol{M_C M_L}$
Similarities	$\boldsymbol{M_D}$	$\boldsymbol{M_D}=\begin{bmatrix}1 & \boldsymbol{D^T}\\ \boldsymbol{D} & \boldsymbol{m_D}\end{bmatrix}$	
	Parameters	$\boldsymbol{M_R}=\boldsymbol{M_L M_C}$: $\theta=\frac{1}{2}\text{atan2}(-(\boldsymbol{M_R})_{13}, (\boldsymbol{M_R})_{23})$ $\boldsymbol{M_R}=\boldsymbol{M_C M_L}$: $\theta=\frac{1}{2}\text{atan2}\left((\boldsymbol{M_R})_{31}, -(\boldsymbol{M_R})_{32}\right)$ $\delta=\cos^{-1}\left(\sqrt{\left((\boldsymbol{M_R})_{11}+(\boldsymbol{M_R})_{22}\right)^2+\left((\boldsymbol{M_R})_{12}+(\boldsymbol{M_R})_{21}\right)^2}-1\right)$ $\alpha=\frac{1}{2}\text{atan2}\left((\boldsymbol{M_R})_{12}-(\boldsymbol{M_R})_{21}, (\boldsymbol{M_R})_{11}+(\boldsymbol{M_R})_{22}\right)$ $\Delta=1-\frac{1}{3}\left[tr\left\lvert\frac{\boldsymbol{M_\Delta}}{(\boldsymbol{M_\Delta})_{00}}\right\rvert-1\right]$ $A=(\lvert\boldsymbol{M_{\Delta 11}}\rvert-\lvert\boldsymbol{M_{\Delta 22}}\rvert)/(\lvert\boldsymbol{M_{\Delta 11}}\rvert+\lvert\boldsymbol{M_{\Delta 22}}\rvert)$	

linear retardance, and depolarization of the whole 50-μm, 100-μm, 200-μm, 300-μm tissue sections obtained by Lu-Chipman and reciprocal polar decompositions of the Mueller matrices measured in backward geometry. The recovery by reciprocal polar decomposition that the orientation angle does not vary with increasing thickness, linear retardance scales close to linearly with thickness, and depolarization increases with thickness in a sublinear fashion is consistent with tissue sections of aligned fibers across the thickness being imaged in our experiments. In contrast, Lu-chipman decomposition fails in producing consistent results for sections of varying thickness.

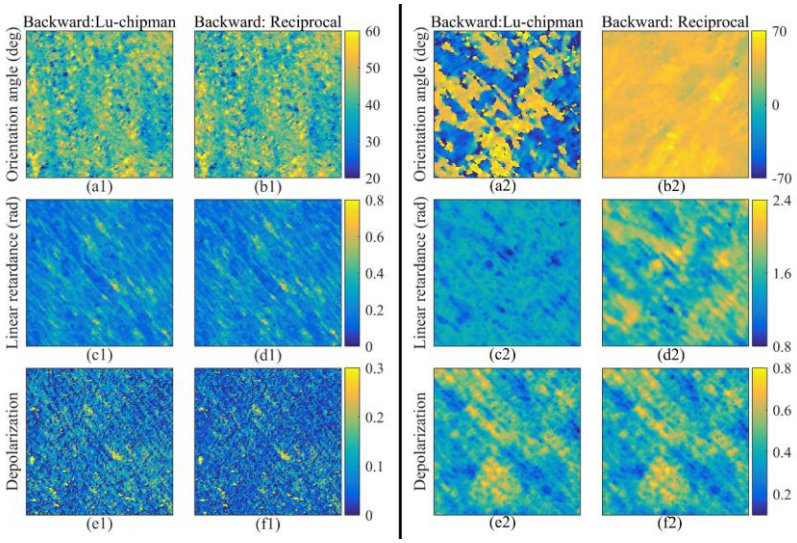

Fig. S1. Polarization imaging of fresh beef tissue sections in serial cuts with thicknesses of 50 µm and 200 µm. The orientation angle, linear retardance, and depolarization: (a1, c1, e1) and (a2, c2, e2) Lu-Chipman decomposition of the Mueller matrix for the 50-µm and 200-µm sections measured in backward geometry; (b1, d1, f1) and (b2, d2, f2) reciprocal polar decomposition of the Mueller matrix for the 50-µm and 200-µm sections measured in backward geometry.

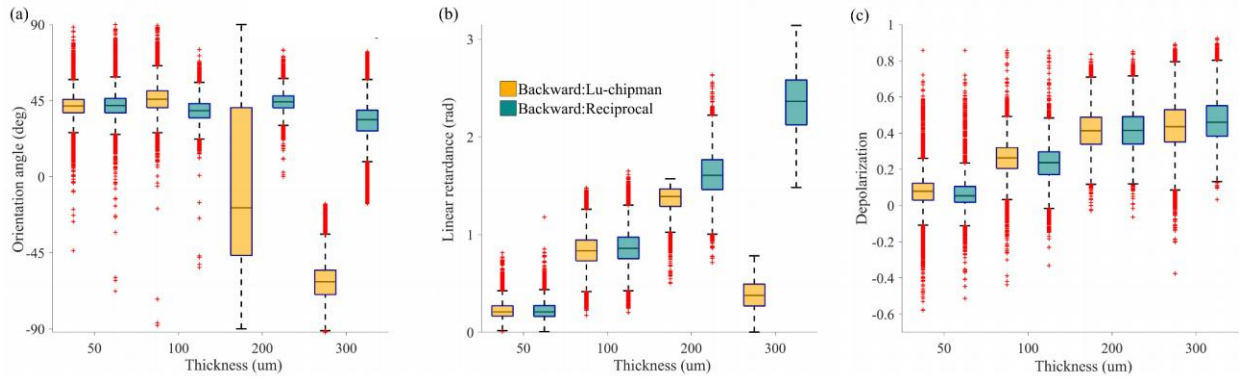

Fig. S2. Boxplots for the orientation angle (a), linear retardance (b), and depolarization (c) of the whole 50, 100, 200, 300-µm beef tissue sections obtained by Lu-Chipman and reciprocal polar decompositions of the Mueller matrices measured in backward geometry.

Supplementary Text 3: Failure of differential decomposition of backscattering Mueller matrices

Differential decomposition assumes that the medium polarization properties are uniform along the optical path [33, 50-52], and the derivative of the Mueller matrix along the optical path, *z*, can be written as

$$\frac{d\boldsymbol{M}(z)}{dz} = \boldsymbol{m}(z)\boldsymbol{M}(z) \tag{S2}$$

where the matrix ***m*** contains the elementary polarimetric properties of the sample per unit of distance (i.e., specific properties).

We analyzed the anisotropy of the birefringence resolution target and beef tissues through differential decomposition. The extracted linear retardance and orientation angle as well as depolarization for the target by differential decomposition in the backward geometry are shown in Fig. S3. Differential decomposition yields incorrect linear retardance and orientation angles (see Table 1 in the main text). The extracted linear retardance, orientation angle, depolarization, and depolarization anisotropy for the fresh beef sections with thicknesses of 100 μm and 300 μm obtained via differential decomposition in the backward geometry are shown in Fig. S4. Differential decomposition in the backward geometry of the 300-μm tissue section produces incorrect orientation angles and retardance. In addition, the linear retardance obtained by differential decomposition of the backscattering Mueller matrix contains sporadic artifacts (see the region outlined by the red line in Fig. S4 (b2)). The linear retardance from the differential decomposition of the backscattering Mueller matrix is multiplied by 1/2 in Figs. S3 and S4 because it accounts for both forward and backward paths.

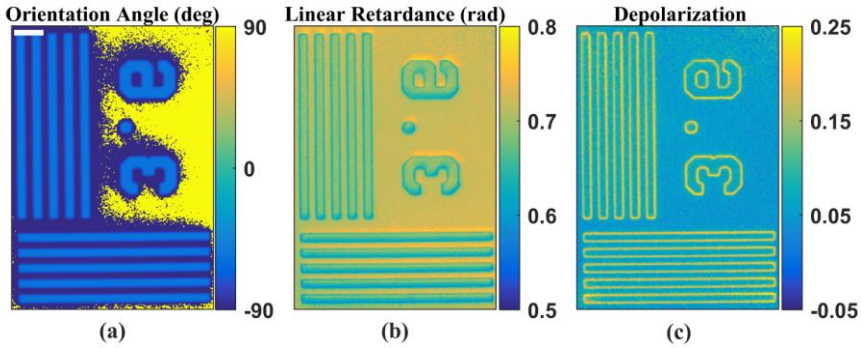

Fig. S3. The orientation angle (a), linear retardance (b), and depolarization (c): differential decomposition of the Mueller matrix for the target measured in the backward geometry. Space bar: 0.5 mm. The orientation angle is off by ~90 degrees, and the linear retardance is ~π/2 smaller than the ground truth (see the correct results in Fig. 3, Table 1).

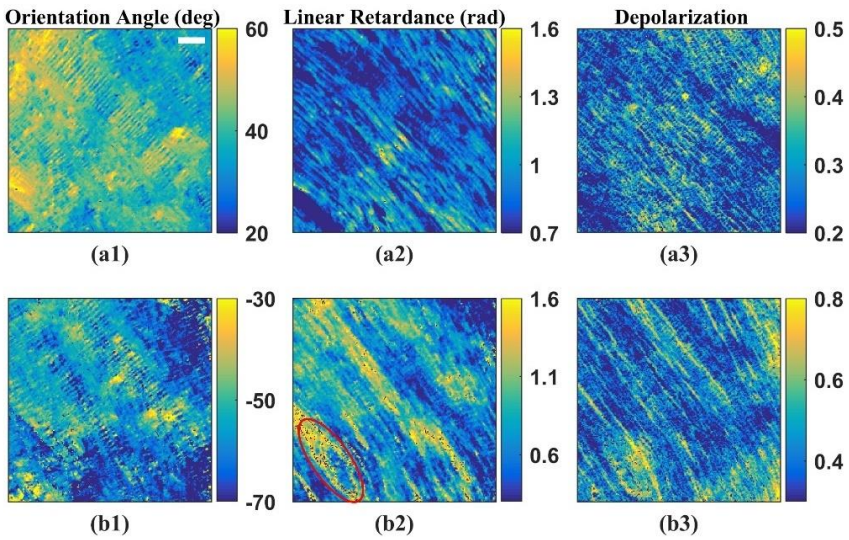

Fig. S4. The orientation angle, linear retardance, and depolarization: differential decomposition of (a1, a2; a3) the 100-μm section and (b1, b2; b3) the 300-μm section measured in the backward geometry. The orientation angles and retardance for the 300-μm tissue section are incorrect. The linear retardance further suffers from sporadic artifacts (the region outlined by the red line in (b2)). Space bar: 0.5 mm.

Supplementary Text 4: Failure of symmetric decomposition of backscattering Mueller matrices

Symmetric decomposition [26] assumes that a Mueller matrix of a sample can be decomposed as

$$\boldsymbol{M} = \boldsymbol{M}_{D2}\boldsymbol{M}_{R2}\boldsymbol{M}_{\Delta}\boldsymbol{M}_{R1}^{T}\boldsymbol{M}_{D1} \tag{S3}$$

where $\boldsymbol{M}_{D1}$ and $\boldsymbol{M}_{D2}$ are the Mueller matrices of the two diattenuators, $\boldsymbol{M}_{R2}$ and $\boldsymbol{M}_{R1}^{T}$ are the Mueller matrices of the two retarders, and $\boldsymbol{M}_{\Delta} = \mathrm{diag}(d_0, d_1, d_2, d_3)$. The diattenuator and retarder matrices, $\boldsymbol{M}_{D}$ ($\boldsymbol{M}_{D1}$ and $\boldsymbol{M}_{D2}$) and $\boldsymbol{M}_{R}$ ($\boldsymbol{M}_{R2}$ and $\boldsymbol{M}_{R1}^{T}$), take the same form as in Lu-Chipman decomposition.

Although reciprocal decomposition may appear similar to symmetric decomposition, they differ fundamentally. Reciprocal polar decomposition strictly enforces reciprocity and can only be applied to backscattering polarimetry. It contains ten degrees of freedom as the backscattering Mueller matrices are inherently constrained ($\boldsymbol{QM}$ is a symmetric matrix). Symmetric decomposition, on the other hand, is a generic Mueller matrix decomposition method and has sixteen degrees of freedom. It does not account for the reciprocity of the backward and forward

paths in backscattering measurements. In addition, $\boldsymbol{M}_{R2}$ and $\boldsymbol{M}_{R1}^{T}$ and $\boldsymbol{M}_{D1}$ and $\boldsymbol{M}_{D2}$ in symmetric decomposition are only the Mueller matrices of retarders and diattenuators without further constraints, while $\boldsymbol{M}_{D}$, $\boldsymbol{M}_{D}^{\#}=\boldsymbol{Q}\boldsymbol{M}_{D}{}^{\boldsymbol{T}}\boldsymbol{Q}$ and $\boldsymbol{M}_{R}$, $\boldsymbol{M}_{R}^{\#}=\boldsymbol{Q}\boldsymbol{M}_{R}{}^{\boldsymbol{T}}\boldsymbol{Q}$ in reciprocal decomposition are, respectively, pairs of recirpocal diattenuator matrices and retarder matrices in the forward and backward paths. This leads to a straightforward and direct interpretation of the polarization characteristics of the sample by reciprocal decomposition.

We also analyze the anisotropy of the birefringence resolution target and beef tissues through symmetric decomposition. The extracted linear retardance and orientation angle as well as depolarization for the target by the symmetric decomposition in the backward geometry are shown in Fig. S5. Both the $\boldsymbol{M}_{R1}$ and $\boldsymbol{M}_{R2}$ matrices obtained through symmetric decomposition yield incorrect linear retardance and orientation angle (see Table 1 in the main text). The extracted linear retardance, orientation angle, depolarization, and depolarization anisotropy for the fresh beef sections of thickness 100 μm and 300 μm by the symmetric decomposition in the backward geometry are shown in Fig. S6. Both the $\boldsymbol{M}_{R1}$ and $\boldsymbol{M}_{R2}$ matrices obtained through symmetric decomposition yield incorrect linear retardance and orientation angle. In addition, the image quality of polarization parameters obtained through symmetric decomposition is much poorer than those obtained by reciprocal polar decomposition (see Fig. 3 and 4 in the main text and Fig. S5 and S6).

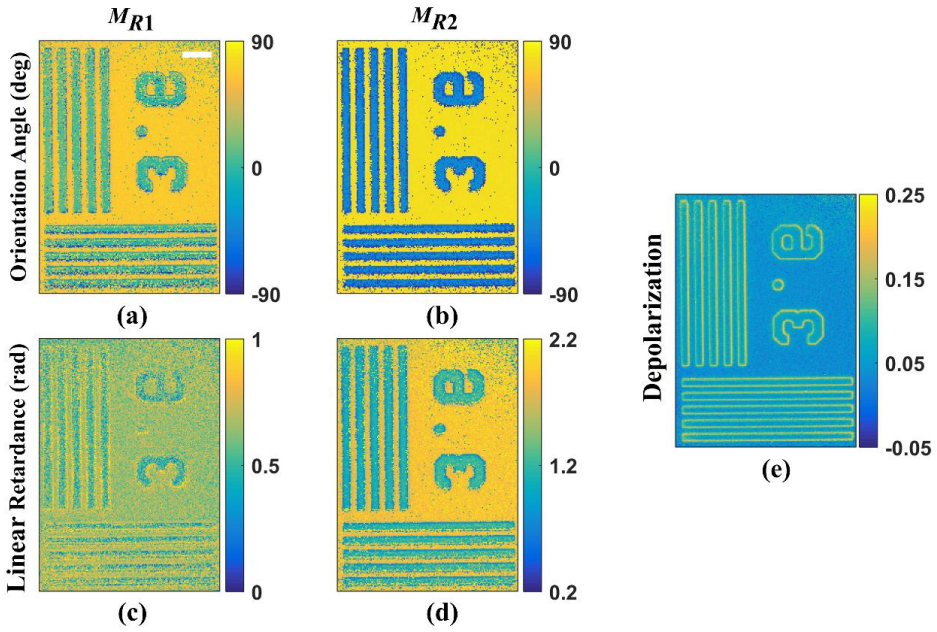

Fig. S5. The orientation angle (a, b), linear retardance (c, d), and depolarization (e): symmetric decomposition of the Mueller matrix for the target measured in the backward geometry obtained from M_{R1} and M_{R2}, respectively. The orientation angle and linear retardance obtained from M_{R1} and M_{R2} differ from each other and are incorrect (see the correct results in Fig. 3, Table 1). The image quality of the polarization parameters is much poorer as well. Space bar: 0.5 mm.

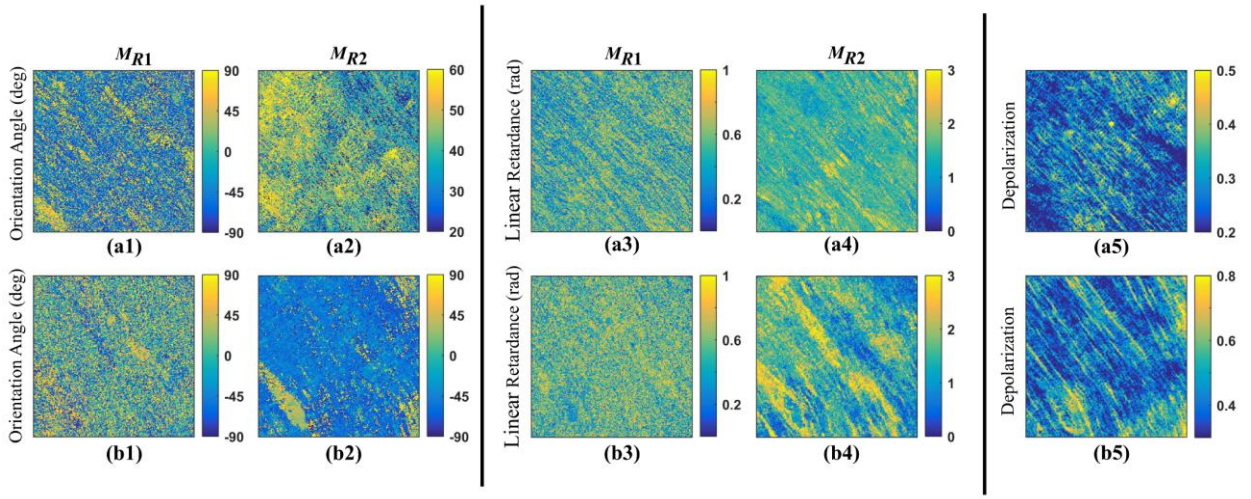

Fig. S6. The orientation angle, linear retardance, depolarization, and depolarization anisotropy: symmetric decomposition of (a1, a2; a3, a4; a5) the 100-μm section and (b1, b2; b3, b4; b5) the 300-μm section measured in the backward geometry. (a1, b1, a3, b3) were obtained from $M_{R1,}$ and (a2, b2, a4, b4) were obtained from M_{R2}. The orientation angle and linear retardance obtained from M_{R1} and M_{R2} differ from each other and are incorrect (see the correct results in Fig. 4). The orientation angles and linear retardances obtained for the 100-μm section and the 300-μm section are inconsistent. Furthermore, the image quality of the polarization parameters is much poorer as well. Space bar: 0.5 mm.

Supplementary Text 5: Comparisons of the polarization properties obtained via Lu-Chipman, differential and reciprocal polar decompositions

Comparisons of the polarization properties obtained by Lu-Chipman and reciprocity polar decomposition are summarized in Table S2. The polarization properties of complex media determined by the reciprocal polar decomposition of the backscattering Mueller matrices are in excellent agreement with those obtained by polarization imaging of the same sample in forward geometry. Reciprocal polar decomposition can recover the optical rotations properly, whereas Lu-Chipman produces erroneous results from backscattering Mueller matrices. In addition, the values of the polarization parameters recovered by reciprocal polar decomposition are more consistent in the data distribution (tighter clustering around the median) and even exhibit sharper contrast between cancerous and normal tissue than the forward measurement. The greater depolarization caused by reciprocal polar decomposition in the backscattering geometry than that caused by Lu-Chipman decomposition in the forward geometry is caused by the different detection geometries.

In contrast, the Lu–Chipman decomposition of the backscattering Mueller matrix produces similar yet distorted retardance, depolarization, and depolarization anisotropy images compared with the reciprocal polar decomposition for media with a retardance less than $\pi/2$ (see Fig. 4). Lu-Chipman decomposition does not obtain the optical rotation correctly in the backscattering geometry. For media with retardance exceeding $\pi/2$, significant errors in the orientation angle and retardance are observed in the Lu–Chipman decomposition of the backscattering Mueller matrices (see Figs. 3, 4, Table 1).

The differential decomposition shows similar but inferior results to those of the Lu-Chipman decomposition in the backward scattering geometry.

Table S2. Comparisons of the polarization properties obtained via Lu-Chipman decomposition and reciprocal polar decomposition. The shaded boxes denote erroneous values.

	Lu-Chipman (forward)	Lu-Chipman (backward)	Reciprocal (backward)
Linear retardance	$\delta\,(\delta < \pi/2)$	$\approx \delta$	$= \delta$
	$\delta\,(\delta > \pi/2)$	$< \delta$	$= \delta$
Orientation angle	$\theta\,(\delta < \pi/2)$	$\approx \theta$	$= \theta$
	$\theta\,(\delta > \pi/2)$	$\approx \theta \pm 90°$	$= \theta$
Depolarization	Δ	$> \Delta$	$> \Delta$
Optical rotation	α	$<<\alpha$	$= \alpha$
The images (δ, θ, Δ, α)		Poor sharpness	Better sharpness